Journal of Neuroinflammation

RESEARCH

Open Access

Extracellular vesicle-derived miR21 of non-tumoral origin as early diagnostic marker of glioma

Mariassunta De Luca[1], Arianna Rinaldi[1], Arianna Ioni[1], Anaïs Oudin[2], Andrea Scafidi[3], Aurélie Poli[3], Laura Vilardo[4], Anna Golebiewska[2], Igea D'Agnano[4], Alessandro Michelucci[3], Cristina Limatola[5,6] and Myriam Catalano[1*]

Abstract

Background Extracellular vesicles (EVs) are key elements in intercellular communication and are released into body fluids by all cells in physiological and pathological conditions. In brain tumors, EVs facilitate the bidirectional communication between neoplastic cells and the tumor microenvironment, promoting tumor progression and immune evasion. Among the various components of the EVs, microRNAs (miRs) act as potent regulators of gene expression. In particular, miR21 has gained attention as both a promising diagnostic biomarker and a key contributor to GBM progression.

Methods This study employed content analysis of miRs in EVs isolated from the brain, plasma, and urine of glioma-bearing mice.

Results Seven days after glioma cell injection, miR21 was the most highly expressed miR in both the brain and biofluids. Notably, its overexpression was particularly prominent in medium/large EVs. Co-culture experiments revealed that the early source of this marker is primarily microglia, rather than tumor cells.

Conclusion These data point out the potential of miR21 as early biomarker for glioma diagnosis and disease monitoring, emphasizing the role of non-tumoral cells, particularly microglia, as rapidly reacting elements in the context of gliomas.

Keywords Extracellular vesicles, MiR21, Glioma, Liquid biopsy, Microglia

Introduction

High-grade glioma is typically diagnosed only after the onset of symptoms, including headache, intracranial hypertension, weakness, motor deficits, epileptic seizures or visual and speech impairments [1–3]. Glioma diagnosis typically involves a combination of non-invasive brain imaging techniques, such as magnetic resonance imaging (MRI), and invasive procedures, like a tissue biopsy [2, 4]. While liquid biopsy is not part of routine clinical practice for glioma, it holds promise as non-invasive approach for early diagnosis, monitoring treatment response and recurrence [5].

Extracellular vesicles (EVs) represent diffuse and crucial players in the physiological mechanisms of intercellular communication [6] and they are released into body fluids by virtually all mammalian cells [7]. Similar to other tumours, in glioma EVs facilitate the communication between cancer cells and the surrounding microenvironment, promoting tumor progression, immune

*Correspondence:
Myriam Catalano
myriam.catalano@uniroma1.it

Full list of author information is available at the end of the article

Graphical Abstract

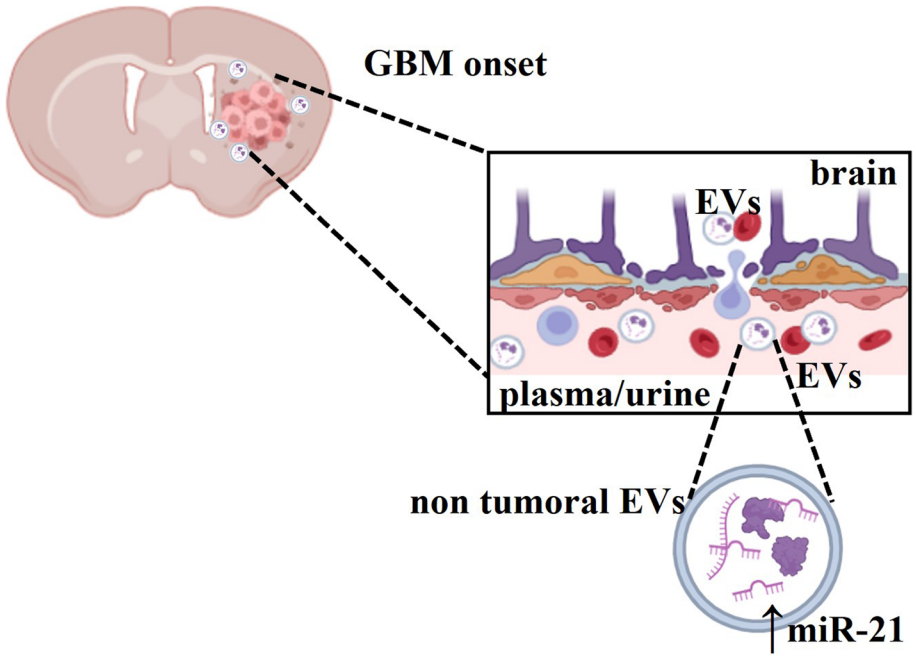

evasion and tissue invasion [8–10]. These vesicles transport proteins, RNA, and other bioactive molecules that influence glioma cell phenotype and contribute to treatment resistance [11–13]. EVs released from brain tumors promote angiogenesis [8], transporting proteins or specific nucleic acids [14] for nitric oxide synthesis and PI3K/AKT signalling into brain endothelial cells [15, 16]. Glioma-derived EVs dampen immune responses transferring immunosuppressive molecules which attenuate T cell activation [17] or promote the formation and expansion of myeloid-derived suppressor cells [18, 19] but also microRNAs (miRNAs) [20–22] and circular RNAs which promote a tumor-supportive phenotype in invading macrophages [23]. Glioma progression is also supported by brain-derived EVs: astrocyte-derived EVs contain PTEN-targeting miRs, which promote glioma growth [24] and brain-originating EVs cross the blood-brain-barrier (BBB) and are detected in the blood and other biofluids [25, 26]. We have recently demonstrated that astrocytic and microglial-derived EVs can modulate tumor microenvironment and glioma cell metabolism in mouse models of the disease [27–29] and we identified miR124 as a mediator of the microglial to glioma communication [29].

Among the miRs linked to cancer progression, miR21 was one of the first to be recognized as oncogenic [30]. miR21 has key roles in malignant processes, affecting genes involved in proliferation, cell survival, invasion, and treatment resistance [31]. Early studies described increased levels of miR21 in primary GBM [32], and miR21 expression is significantly increased in the CSF of GBM patients showing an inverse correlation with the survival rate [33]. Notably, miR21 has been shown to play a pivotal role in the initiation of the carcinogenesis. In various tumor types it promotes cell proliferation by targeting tumor suppressor genes such as programmed cell death protein 4 (2*PDCD4*) [34], sprouty RTK signaling antagonist 2 (*SPRY2*) [35], phosphatase and tensin homolog (*PTEN*) [36], and reversion-inducing cysteine-rich protein with Kazal motifs (*RECK*) [37]. Additionally, miR21 contributes to the inhibition of apoptosis by downregulating key pro-apoptotic factors [38] including apoptotic protease-activating factor 1 (*APAF1*), caspase 3 (*CASP3*), Fas ligand (*FASLG*), and Ras homolog family member B (*RHOB*). Beyond its role in tumor cell survival, miR21 also fosters an immunosuppressive microenvironment through its targets PDCD4 and PTEN [39] as well as Runx1 [40].

While an association of miR21, miR181c, miR195, and miR196b with GBM progression has been reported [41], it remains unclear whether these or other mRNAs contained in EVs serve as reliable biomarkers for early diagnosis or relapse prediction. In addition to its role in tumor progression, miR21 participates in communication with the tumor-microenvironment: in glioma-associated microglia, it favours tumour suppressor activity [42–44] while in endothelial cells it supports angiogenesis [45].

In the current study, we analysed the miR content of EVs isolated from the brain and biofluids (plasma and

urine) of glioma-bearing mice and demonstrated an early increase of miR21 in EVs, largely deriving from non-tumor cells, microglia, and a late production from glioma cells. These findings highlight the potential of miR21 as an early, non-invasive biomarker for glioma detection and monitoring, opening new clinical perspectives for liquid biopsy applications and targeted therapeutic interventions.

Methods

Cell lines

Murine glioma GL261, human GBM U87MG and mouse microglial BV2 cells were cultured in DMEM (Thermo Fisher Scientific, Waltham, MA, USA), supplemented with heat-inactivated FBS (20% for GL261, 10% for U87MG and BV2, Thermo Fisher Scientific, Waltham, MA, USA), 100 IU/mL penicillin G (Thermo Fisher Scientific, Waltham, MA, USA), 100 µg/mL streptomycin (Thermo Fisher Scientific, Waltham, MA USA), 2.5 µg/mL amphotericin B (Thermo Fisher Scientific, Waltham, MA, USA) and grown at 37 °C in a 5% CO2 and humidified atmosphere. FBS was subjected to all centrifugation steps used for EV isolation (see below) to obtain EV-depleted FBS. EV-depleted FBS was used to harvest the EVs. To prepare the GL261-conditioned medium (GCM), GL261 cells were seeded 5×10^5 in a 6-well plate, mock-transfected or transfected with the miR21 inhibitor sequence, as later described in the "Cell transfection" subparagraph and after 24 h culture medium was collected. GCM was used to treat BV2 and primary glial cells for 24 h.

Animals

Eight-week-old male C57BL6/N or immunodeficient SCID mice were used for vehicle and glioma cell injections. GL261 cells (1×10^5 in 4 µl PBS) or U87MG cells (5×10^4 in 4 µl PBS) were inoculated in the right striatal brain region (+ 1 mm anteroposterior, −2 mm lateral from the bregma) of C57BL6/N or immunodeficient SCID mice respectively; cell suspension was injected at 1 µl/min and 3 mm depth. Mice were randomly divided between control group (PBS vehicle injection) and glioma-bearing mice (GL261 or U87MG cells injection). Control group is defined as T0. Glioma-bearing mice group is defined T7, T14 or T21 depending on days after tumor cell inoculation. Eight-week-old female nude mice were implanted with patient-derived orthotopic xenografts (PDOXs) from GBM patients [46]. Nude mice developed intracranial tumors at endpoint showing an invasive (PDOX P8) or angiogenic (PDOX P13) growth pattern [47]; healthy nude mice were used as matched control.

C57BL6/N and immunodeficient SCID mice were housed in standard cages; nude mice were housed in individual ventilated cages (IVC) in SPF conditions. All mice were housed under controlled temperature (20–22 °C), relative humidity (50–55%), 12-h light/dark cycle (7 am – 7 pm) with food and water ad libitum.

For urine collection, each mouse was kept in a single metabolic cage for 24 h, under standard temperature (20–22 °C) and humidity (50–55%) conditions and urine were gathered in a tube at the bottom of metabolic cage. Urine samples (400–1400 µl per mouse) were immediately centrifuged to obtain EVs as later described in the "Extracellular vesicles extraction from plasma and urine" subparagraph.

At different time points (7, 14 or 21 days after tumor cell inoculation), mice under deep anaesthesia (Zoletil 50 mg/Kg plus Rompun 10 mg/Kg intraperitoneally) were blood sampled, through cardiac puncture in EDTA containing tubes to avoid coagulation, then sacrificed to isolate the brain. For plasma preparation, tubes were centrifuged at 1300 g for 15 min at 4 °C. Nude mice were deeply anesthetized with ketamine 100 mg/Kg plus xylazine 10 mg/Kg intraperitoneally, plus buprenorphine 0.05 mg/Kg subcutaneously. Blood was collected through cardiac puncture in EDTA containing tubes, then centrifuged at 12,000 rpm for 30 min at 4 °C. After centrifugation, plasma (30–200 µl) was carefully transferred in new tubes and stored at −80 °C until EV extraction.

All procedures on mice were approved by Italian Ministry of Health (protocol number: 775/2020), by the Luxembourg Ministry of Agriculture and the Luxembourg Ministry of Health (protocols: LRNO-2017-01/LUPA2019/93) in accordance with ethical guidelines on the use of animals from European Communities Council Directive 2010/63/EU and with the Italian D. Lgs 26/2014 and in compliance with the Luxembourg national regulations of the 'Animal Welfare Structure' of the Luxembourg Institute of Health. The ARRIVE guidelines were applied for result reporting.

For PDOXs, GBM patients provided informed consent, and the collection of tumor samples and all experimental procedures were approved by the Haukeland University Hospital, Bergen, Norway under the protocol number 2009/117.

Primary glial cultures

Primary glial cultures (microglia and astrocytes) were obtained from the brain cortex of mouse pups (post-natal day 0–1) as previously described [48, 49]. Briefly, cortices were chopped and digested in 15 U/mL papain (Sigma-Aldrich, Darmstadt, Germany) at 37 °C for 20 min. Cells (5×10^5 cells/cm^2) were plated on flasks coated with poly-L lysine hydrobromide (0.1 mg/mL; Sigma-Aldrich, Darmstadt, Germany). Cells were cultured in DMEM (Thermo Fisher Scientific, Waltham, MA, USA), supplemented with 10% heat-inactivated FBS (Thermo Fisher

Scientific, Waltham, MA, USA), 100 U/mL penicillin G (Thermo Fisher Scientific, Waltham, MA, USA), 100 µg/mL streptomycin (Thermo Fisher Scientific, Waltham, MA USA), 2.5 µg/mL amphotericin B (Thermo Fisher Scientific, Waltham, MA, USA) and grown at 37° C in a 5% CO_2 and humidified atmosphere. After 9–11 days, cells were shaken for 2 h at 37 °C to detach and collect microglial cells. Astrocytes which remained attached on the bottom of the flask were treated with trypsin and collected. Both microglia and astrocytes were seeded 1×10^5 cells in 12-well plate and after 24 h treated with GCM. For the treatment, the culture medium of microglia and astrocytes was replaced with GCM for 24 h.

Cell transfection

GL261 cells (1×10^5) plated onto 6-well plates were mock-transfected or transfected with the miR21 inhibitor sequence (Thermo Fisher Scientific, Waltham, MA, USA) via Lipofectamine 3000 Reagent (Thermo Fisher Scientific, Waltham, MA, USA) in Opti-MEM (Thermo Fisher Scientific, Waltham, MA, USA) according to manufacturer's instructions.

Tumor volume analysis

Mice were deeply anaesthetized with Zoletil (50 mg/Kg) plus Rompun (10 mg/Kg) (i.p.) before intracardiac perfusion with ice-cold PBS and 4% paraformaldehyde (PFA, Santa Cruz Biotech, Dallas, USA). Brain samples were isolated and processed for histological staining. Brains were fixed in 4% PFA for 24 h at 4 °C, cryopreserved in 30% sucrose dissolved in 1x PBS for 48 h at 4 °C and then frozen in 2-metilbutane (Merck, Darmstadt, Germany) for 24 h at −80 °C and embedded in optimal cutting temperature (OCT, Bio Optica, Milano, Italy) compound. Serial 20 µm coronal brain slices were cut using Cryostat Leyca and stained with a haematoxylin-eosin staining standard protocol. Brain slices were analysed by the Image Tool 3.0 Software (University of Texas, Health Science Center, San Antonio, TX, USA). Tumor area was calculated according to the formula (volume = t x ΣA), where A is the tumor area/slice and t is the thickness.

Extracellular vesicle extraction from cells

Prior to extracellular vesicle extraction, the culture medium of BV2, microglial, and astrocytic cells was replaced with fresh medium and incubated for 24 h to ensure standardized EVs release conditions. Cell supernatant was collected and centrifuged at 800 g for 5 min to remove cell debris. The supernatant was centrifuged at 10,000 g for 30 min at 4 °C to obtain the medium/large EVs (m/lEVs)-containing pellet. The pellets were re-suspended in a 0.22 µm filtered PBS for NTA and Resuspension Buffer (50 µl, Thermo Fisher Scientific, Waltham, MA, USA) for RNA and protein extraction. The EVs-free fraction medium was used as control.

Extracellular vesicle extraction from brain tissue of glioma-bearing and control mice

To isolate EVs from brain of GL261-injected and control C57BL6/N mice, a modified protocol from Crescitelli et al. was used [50]. Briefly, after a deep anaesthesia, mice were sacrificed and brain tissues were collected in a tissue dish with DMEM + Hepes 20 mM (Thermo Fisher Scientific, Waltham, MA, USA) to be cut in small pieces (2 mm x 2 mm x 2 mm). Then, in a 6-well plate, medium was supplemented with DNase I (Invitrogen, Thermo Fischer Scientific, Waltham, MA, USA) and collagenase D (Roche, Basel, Switzerland) at a final concentration of 40 U/mL and 2 mg/mL respectively. After an incubation with enzymes on a nutating mixer under mild agitation (30 rpm) for 30 min at 37 °C, medium was filtered on sterile 70 µm cell strainer on top of a 50 mL tube and was centrifuged at 300 g for 10 min at 4 °C. Carefully, the supernatant was transferred in a new tube and was centrifuged at 2000 g for 20 min at 4 °C. The obtained supernatant was centrifuged at 16,500 g for 20 min at 4 °C. The resulting pellet, containing m/lEVs, was resuspended in 100 µL 0.22 µm filtered 1x PBS w/o Ca^{2+}/Mg^{2+} for NTA or Resuspension buffer (Thermo Fisher Scientific, Waltham, MA, USA) for RNA and protein extraction. The supernatant was transferred in a new tube and was ultracentrifuged at 100,000 g for 2.5 h at 4 °C and the resulting pellet, containing sEVs, was resuspended in 100 µL 0.22 µm filtered 1x PBS w/o Ca^{2+}/Mg^{2+} for NTA analysis or in 100 µL of Resuspension Buffer (Thermo Fisher Scientific, Waltham, MA, USA) for RNA isolation and western blot analysis.

Extracellular vesicle extraction from plasma and urine of glioma-bearing and control mice

Plasma of GL261-injected and control C57BL6/N mice and of U87-injected and control SCID mice and urine of GL261-injected and control C57BL6/N mice were used to isolate EVs, by using a modified protocol from Théry et al. [51]. Briefly, tubes containing plasma or urine were subject to two subsequently centrifugations (the first at 2000 g, 20 min, 4 °C; the second at 12,000 g, 45 min, 4 °C) and the resulting pellet was washed 2 times with PBS (w/o Ca^{2+}/Mg^{2+}, 0.22 µm-filtered). The pellet contained m/lEVs; the supernatant was ultracentrifuged 2 times (100,000 g, 1 h, 4 °C) to obtain sEVs. Pellets were resuspended in 100 µl 0.22 µm filtered PBS w/o Ca^{2+}/Mg^{2+}, for NTA analysis or in 100 µl of the Resuspension Buffer (Thermo Fisher Scientific, Waltham, MA, USA) for RNA isolation and western blot analysis. Plasma was also obtained from healthy nude mice, nude mice with PDOX

P8 or with PDOX P13 and, for EVs isolation, the protocol described previously was used.

Nanoparticle tracking analysis (NTA)

EVs were analysed using Nanosight NS300 (Malvern Panalytical, Malvern, UK) at room temperature (22–25 °C). The samples were diluted in PBS (w/o Ca^{2+}/Mg^{2+}, 0.22 µm-filtered) to a final volume of 1 mL, obtaining an optimal particle range (20–100) per frame, 30 frames per sec. Videos, taken with the sCMOS camera with set level 14 and detection threshold 4, were analyzed by the inbuilt NanoSight Software NTA 3.4 Dev Build 3.4.4. For each sample, 5 measurements (60 s movie each) were done. EVs concentration is reported as number of particles/mL.

Western blot

EVs were lysated in Resuspension buffer and the total protein level was quantified by BCA assay (Thermo Fisher Scientific, Waltham, MA, USA). The same amount of protein per sample (20 µg) resuspended in Laemmli sample buffer (125 mM Tris HCl pH6.8, 4% SDS, 20% glycerol, 200 mM DTT, 140 µM bromophenol blue) sonicated and boiled at 100 °C for 5 min. Protein samples were separated by 12% SDS-polyacrylamide gel electrophoresis and transferred onto nitrocellulose membrane. The membrane was blocked for 45 min in 5% (w/v) non-fat dry milk in TBS-T buffer (0.1% Tween-20 in 0.1 M Tris-Buffered Saline). Then, the membrane has been cut probing different regions of the same blot with the primary antibodies rabbit anti-CD81 (1:500, Cell Signaling, Danvers, MA, USA) and rabbit anti-TSG101 (1:500, GeneTex, Irvine, CA, USA) (in 3% (w/v) non-fat dry milk TBS-T, at 4 °C overnight). After three washes with TBS-T for 10 min, membranes were incubated with the HRP-tagged goat anti-rabbit secondary antibody (1:3000, Dako, Cernusco sul Naviglio, Italy), in 1% (w/v) non-fat dry milk TBS-T, 2 h at room temperature. The detection was performed through the chemiluminescence assay with the Amersham ECL PrimeWestern Blotting Detection reagent (Cytiva, Little Chalfont Buckinghamshire, UK) by a ChemiDoc Imaging System (Bio-Rad, Hercules, CA, USA).

RNA extraction and quantitative RT-PCR

Total RNA was extracted from EVs with Total EXO RNA Extraction Kit (4478545, Thermo Fisher, Waltham, MA, USA) according to manufacturer's instructions. RNAs extracted from all samples were quantified and reverse-transcribed using TaqMan MicroRNA reverse transcription kit (Applied Biosystems, Foster City, CA, USA) according to the manufacturer's recommendations. For quantitative PCR, TaqMan Universal Master Mix II, no UNG (Applied Biosystem, Foster City, CA, USA) was used together with the following miRNA assays: snU6, ID 001973; hsa-miR21, ID 000397; hsa-miR222, ID 002276 for specific murine sequences; snU6, ID 001093; hsa-miR21, ID 002438 for specific human sequences. The PCRs were performed on a CFX96 Dx System (Bio-Rad) and the following two-step cycler profile: 50 °C for 2 min, 95 °C for 10 min, 40 cycles of denaturation at 95 °C for 15 s and annealing/extension at 60 °C for 1 min. The PCRs for PDOX model's samples were performed in a 384-well on a Quantstudio5 (Applied Biosystem, Thermo Fisher Scientific, Waltham, MA, USA) using the standard programme described above. SnU6 was used as endogenous control for normalization and the relative miRNAs quantities were calculated with the $2^{-\Delta Ct}$ method for in vivo experiments (target gene expression in samples from different individuals) and with $2^{-\Delta\Delta Ct}$ method for in vitro experiments (target gene expression in samples subjected to different treatments) [52].

MiRNA sequencing

miRNA profiling was carried out on total RNA (extracted as described above) and the libraries were prepared and sequenced by a certified sequencing hub. The workflow included sample quality control, library preparation, final QC, and sequencing performed on Illumina NextSeq/NovaSeq platforms using 2×40 bp paired-end reads, with a throughput of approximately 40 million paired-end reads per sample and a Q30 score of 85%, ensuring high-quality data. The samples were analysed using miRNA platform, miRXes (Singapore, China). FASTQ files were assessed for quality control with Fastp (v0.20.1). The reference genome (GRCh38) was used for mapping the RNA sequencing libraries, using annotation subset for miRNA only. The specific aligner used for mapping was BWA (version 0.7.17), downstream processing was performed using R (version 4.2.1). The alignment file in SAM format was converted to the BAM format and miRNA read counts were assigned using Subread feature Counts. FPKM (Fragments Per Kilobase per Million) values were calculated using base R functions. Differentially expressed miRNAs were identified based on fold-change (FC) > 5 and a log2 FC thresholds were used to assess up- or down-regulation.

Statistical analysis

All data were expressed as mean ± SEM and displayed as individual dots. Statistical difference was determined by unpaired t-test or one-way analysis of variance (ANOVA). A value of $p < 0.05$ was considered significant. Normality test was considered passed with alpha = 0.05. Statistical analysis was performed using GraphPad version 8.0 software.

Results

EV concentration correlates with tumor volume in glioma-bearing mice

We investigated the presence of EVs in brain and in plasma of C57BL6/N mice injected with GL261 or control animals. Both medium/large EVs (m/lEVs) and small EVs (sEVs) were detected, and size distribution and dimension were investigated by nanoparticle tracking analysis (NTA) (Fig. 1A and Fig. S1A). A mean size above 150 nm is observed for m/lEVs (brain: 220 ± 5 nm; plasma: 230 ± 8 nm) and below 150 nm for sEVs (brain: 80 ± 5 nm; plasma: 90 ± 8 nm), with a net distribution around the mean for the brain-derived EVs (190 ± 2 nm for m/lEVs and 150 ± 1 nm for sEVs) and a more scattered distribution for plasma-derived EVs (90 ± 15 nm for m/lEVs and 100 ± 18 nm for sEVs) (Fig. 1A, Fig. S1A). The expression of bona fide vesicle marker (CD81 and TSG101) both in brain and plasma derived EVs was verified by Western blotting (Fig. 1B). Altogether these data confirm the specificity of EV isolation.

The concentration of EVs does not differ at early tumour stage (T7 vs. T0) but significantly increases later for both brain- and plasma-derived EVs (T21 vs. T7, Figs. 1C, D, Fig. S1B) and a positive correlation is observed between tumor volume and EV concentration (both m/lEVs and sEVs) (Figs. 1E-H, Fig. S1C).

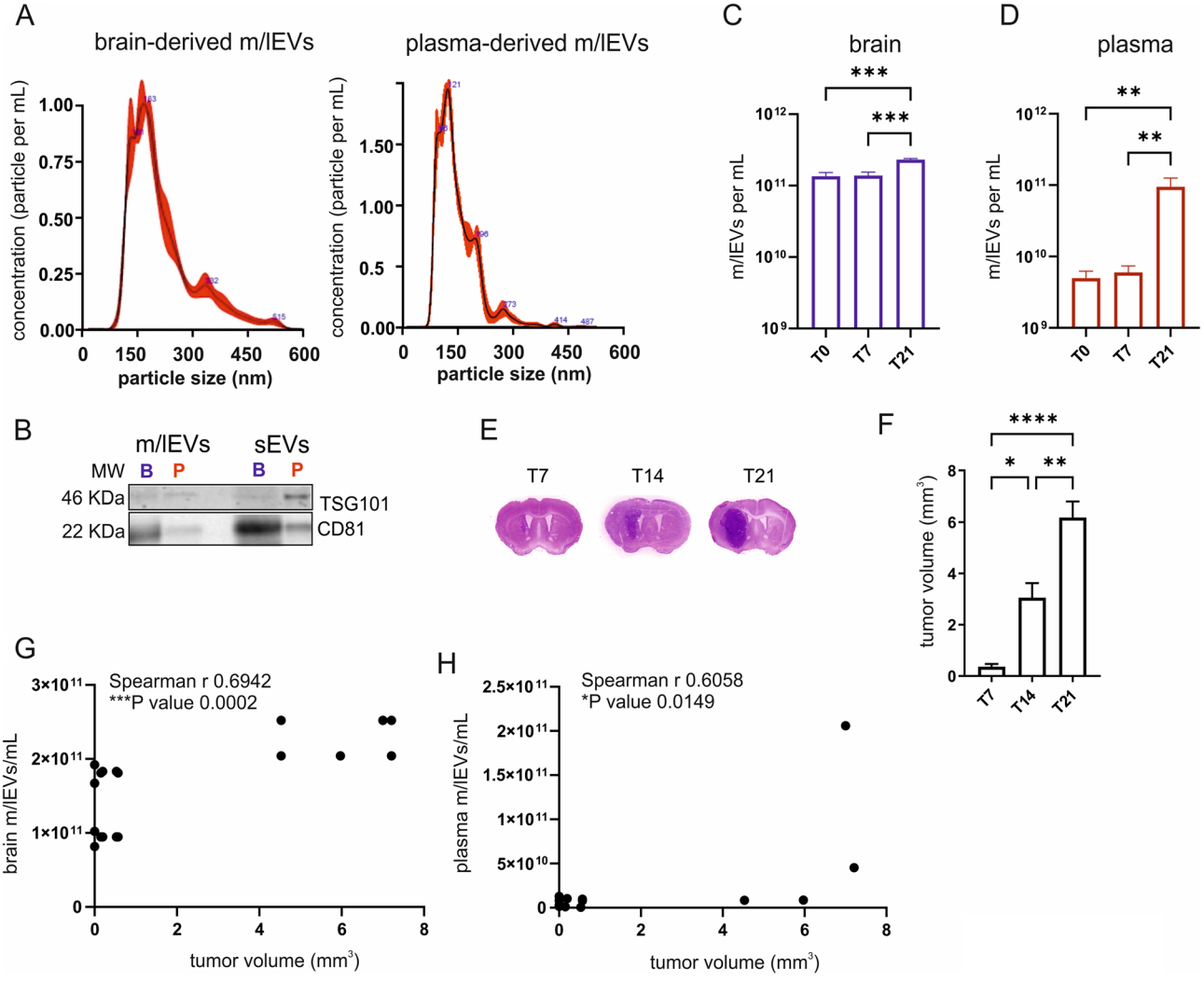

Fig. 1 m/lEVs analysis in brain and plasma of GL261-bearing mice. **A** Representative concentration/size graph from the nanoparticle tracking analysis (NTA). The average concentration (mean ± SE; in particles/mL) and mean size (± SE; in nm) of m/lEVs isolated from brain (left) and plasma (right) of GL261-bearing mice. **B** Western blotting on m/lEVs and sEVs isolated from brain (B) and plasma (P) of GL261-bearing mice, CD81 and TSG101 are used as typical EVs markers. **C-D** Quantification of m/lEVs isolated from brain and plasma time dependent. Data are reported as mean ± SEM, $n = 4$ independent experiments, ANOVA one-way, Tukey's post-hoc analysis, *** $p < 0.001$, ** $p < 0.01$. **E** Representative coronal sections of GL261-bearing mice 7, 14 and 21 days of inoculation (T7, T14, T21). **F** Analyses of tumor size (mm^3) at T0, T7 and T14 is reported as mean ± SEM, $n = 3$–4/experimental groups, ANOVA one-way followed by Bonferroni multiple comparison test, * $p < 0.05$, ** $p < 0.001$, **** $p < 0.0001$; **G-H** Concordance between tumor size and the m/lEV release in brain and plasma identified using Spearman nonparametric correlation analysis; two-tailed p values and *r* correlation coefficients are indicated

miR21 expression in EVs of glioma bearing mice

EVs are an extraordinary tool to exchange material among cells. To investigate potential new biomarkers of glioma, we investigated the miRNAs content of EVs identified in brain and plasma of glioma bearing mice for their high impact on many cellular functions [53]. Taking advantage of the MiRXES platform, we detected 1484 miRNAs out of 1879 analysed in brain-derived m/lEVs. The analyses of these miRNAs revealed that 225 genes were common for all time points analysed (Fig. 2A), likely indicating a constitutive, glioma independent expression. To investigate miRNA expression changes with time, we analysed the differential expression between T0 and T7 (Fig. 2B, x-axis) and between T7 and T21 (Fig. 2B, y-axis), identifying a group of genes that increases early in the presence of cancer (Fig. 2B, quadrant I). Among these genes, we considered only those with a Fragments Per Kilobase per Million (FPKM) greater than 10,000 and quantified the increase at T7, to identify early tumour markers. This analysis revealed that miR21 and miR222 have the greatest increase (Fig. 2C); qRT-PCR analysis confirmed early significant increase of miR21 and miR222 in brain-derived m/lEVs, which is maintained significant at later time points only for miR21 (Fig. 2D). In brain-derived sEVs, 1527 miRNAs out of 1879 analysed were found. The number of miRNAs carried by sEVs increased with tumour progression, with 368 unique genes at T0, 381 unique genes at T7 and 427 unique genes at T21. A core group of 315 genes was expressed at all time points analysed (Fig. S2A). At difference with the m/lEVs, in the sEVs, although miR21 and miR222 were among the genes that increase earlier in the presence of tumour (Fig. S2B, quadrant I), the most expressed genes (with FPKM greater than 10000) at T7 (vs. T0) were the onco-suppressors miRLET7C and miRLET7G (Fig. S2C). qRT-PCR analyses at T0, T7 and T21 show no significant variations over time for miR21 and miR222 in sEVs (Fig. S2D).

In parallel, plasma m/lEVs and sEVs isolated from glioma-bearing mice were analysed by MiRXES at T0, T7 and T21 (Fig. 2E and Fig. S2E). We found 1243 genes expressed out of 1879 analysed in plasma m/lEVs (Fig. 2E). Among the miRNAs that increase early in the presence of cancer (Fig. 2F, quadrant I) (FPKM > 10000) miR21 was the most expressed (Fig. 2G). qRT-PCR analysis at T0, T7, and T21 revealed an early significant increase of miR21 in plasma-derived m/lEVs, which persisted with time (Fig. 2H). Similarly, within the sEV subpopulation, the total number of miRNAs carried by plasma-derived vesicles did not increase with tumor progression (Fig. S2E). Among the miRNAs that showed early upregulation in the presence of cancer (Fig. S2F, quadrant I), only those with an FPKM greater than 10,000 were considered. At T7, miR23A and miR191 were the most highly expressed (Fig. S2G). Notably, miR21 and miR222 were not included in this selection, and qRT-PCR analysis confirmed that their levels did not significantly change over time in plasma-derived sEVs (Fig. S2H). These analyses show that at T7, brain- and plasma-derived m/lEVs express high levels of miR21.

To investigate whether this expression was limited to these two compartments, EVs were also isolated from the urines of GL261-bearing mice at T0, T7 and T21. NTA and western blot analysis of sEVs and m/lEVs confirmed the expected size distribution and molecular profile (Figs. 3A, B). A positive correlation between tumor volume and urine EVs concentration is observed for the m/lEV type (Fig. 3C). The concentration of m/lEVs isolated from urine was similar at T0 and T7, and significantly increased at longer time point, while sEVs concentration significantly increased earlier (Fig. 3D). Analysis of the EV-associated miRNAs showed an increased expression of miR21 only in m/lEVs at T7 (Fig. 3E).

miR21 is early released by EVs derived from non-tumoral cells

It has been reported that glioma cells transfer miR21 to microglial cells through EV release, with effects on microglial phenotype [44]. To identify the early source of miR21 in our experimental setting, we used a xenogeneic glioma model to recognise mouse (host) and human (tumor) miRNAs. We inoculated human GBM cells (U87MG) into the brain striatal region of SCID mice and isolated brain and plasma m/lEVs at T0, T7 and T21. NTA analysis revealed a mean size of 220.2 ± 3.1 nm and 158.7 ± 2.6 nm respectively for brain- and plasma-derived m/lEVs (Fig. 4A). Similar to the syngeneic mouse model of glioma (see Figs. 1C and D), the concentration of m/lEVs isolated from both the brain and plasma did not change at early tumour stage (T7 vs. T0), while it significantly increased at advanced stages (T21 vs. T7) (Fig. 4B). qRT-PCR analysis with specie-specific probes revealed that miR21 in brain and plasma m/lEVs derives only from mice (host) at T7 (Figs. 4C, D). We also investigated the presence of murine and human miR21 in m/lEV obtained from plasma of PDOX model mice injected with two different patient-derived tumoroids. As shown in Figure S3A m/lEVs obtained from plasma of healthy, PDOX P8 and PDOX P13 nude mice and analysed by NTA showed a mean size above 150 nm (healthy: 220 ± 5 nm; PDOX P8: 207 ± 7 nm; PDOX P13: 196 ± 3 nm), with a net distribution around the mean for the PDOX EVs (188 ± 12 nm for PDOX P8 and 150 ± 1 nm for PDOX P13) and a more scattered distribution for healthy EVs (196 ± 2 nm). Data shown in Fig. S3B demonstrate that at least at late stages (T > 21) there is no significant variation in the amount of either mouse or human miR21. Note that these tumors have different growth speed and for this reason we could

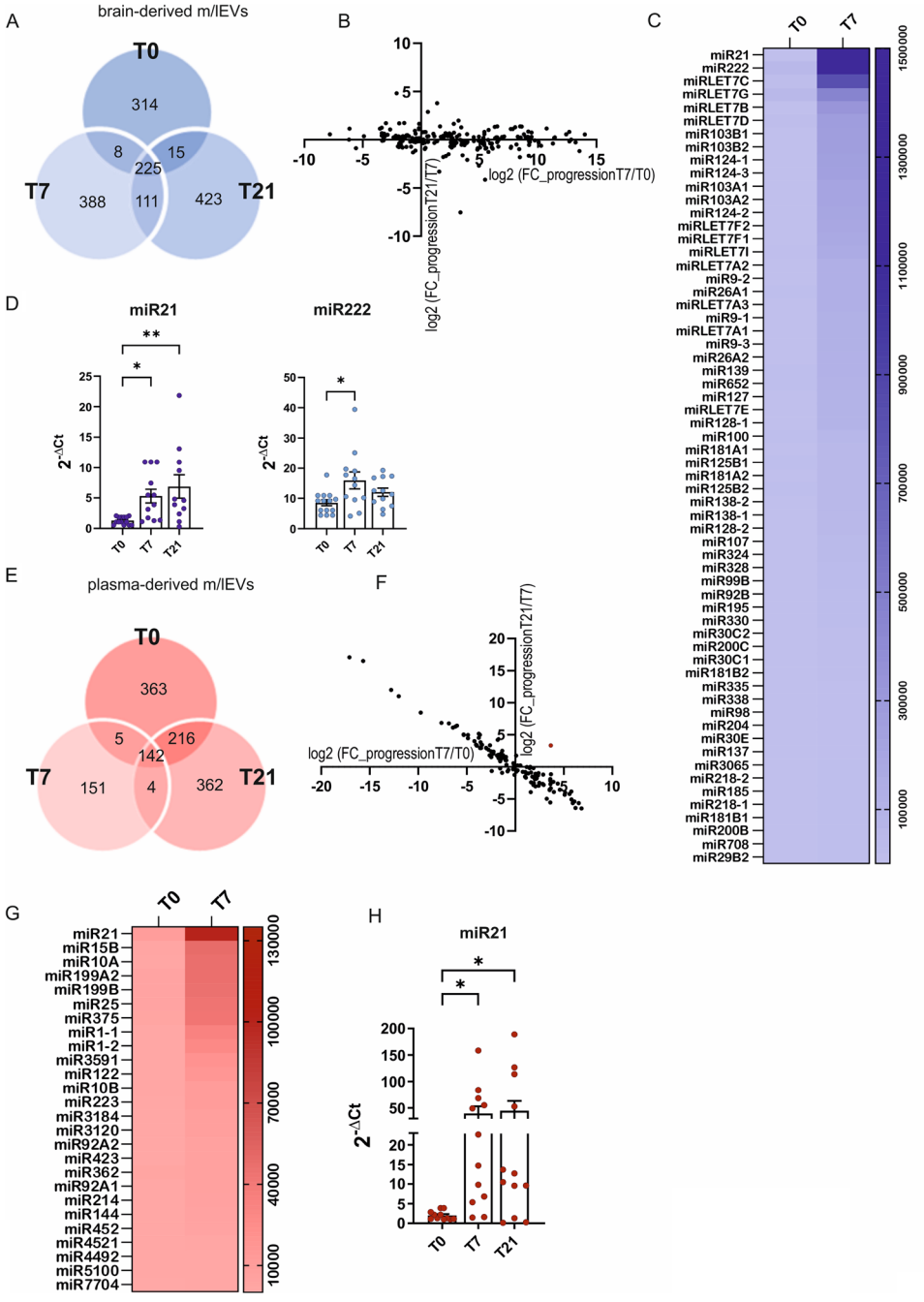

Fig. 2 miRs analysis in m/lEVs from brain and plasma of GL261-bearing mice. **A** Venn diagram of the number distribution of brain m/lEVs-derived miRNAs at T0, T7 and T21 from tumor injection. **B** Scatter plot of differential miRNA expression log2 (FC, fold change) at T7 vs. T0 (x-axis) and T21 vs. T7 (y-axis). In quadrant I, miRNAs upregulated at T7 vs. T0 and at T21 vs. T7; quadrant II, upregulated at T7 vs. T0 and downregulated at T21 vs. T7; quadrant III, downregulated at T7 vs. T0 and at T21 vs. T7; quadrant IV, downregulated at T7 vs. T0 and overexpressed at T21 vs. T7. **C** Heatmap showing the genes selected in panel B, quadrant I, with FPKM > 10,000 at T7. **D** Quantitative real-time PCR of miR21 and miR222 expression in brain m/lEVs at different time points (T0, T7, T21). Each sample has been normalized to U6 snRNA. Data were expressed as the mean ± SEM of $2^{-\Delta Ct}$, T0 = 12–14 animals, T7 = 12 animals, T21 = 11–12 animals. Data were analyzed with ANOVA one-way, Tukey's post-hoc analysis, $*p < 0.05$, $**p < 0.001$. **E** Venn diagram of the distribution of the number of plasma m/lEVs-derived miRNAs at T0, T7 and T21 tumor injection based on FPKM values. **F** Scatter plot of differential miRNA expression log2 (FC, fold change) of miRNA expression at T7 vs. T0 (x-axis) and T21 vs. T7 (y-axis). In quadrant I, miRNA overexpressed at T7 vs. T0 and T21 vs. T7; II, overexpressed at T7 vs. T0 and downregulated at T21 vs. T7; III, downregulated at T7 vs. T0 and T21 vs. T7; IV, downregulated at T7 vs. T0 and overexpressed T21 vs. T7. **G** Heatmap showing the genes selected in panel F, quadrant I, with FPKM > 10,000 at T7. **H** Quantitative real-time PCR of miR21 expression in plasma m/lEVs at different time points (T0, T7, T21). Each sample has been normalized to U6 snRNA. Data were expressed as the mean ± SEM of $2^{-\Delta Ct}$, T0 = 11 animals, T7 = 12 animals, T21 = 12 animals. Data were analyzed with ANOVA one-way, Tukey's post-hoc analysis. Differences were considered statistically significant as $*p < 0.05$

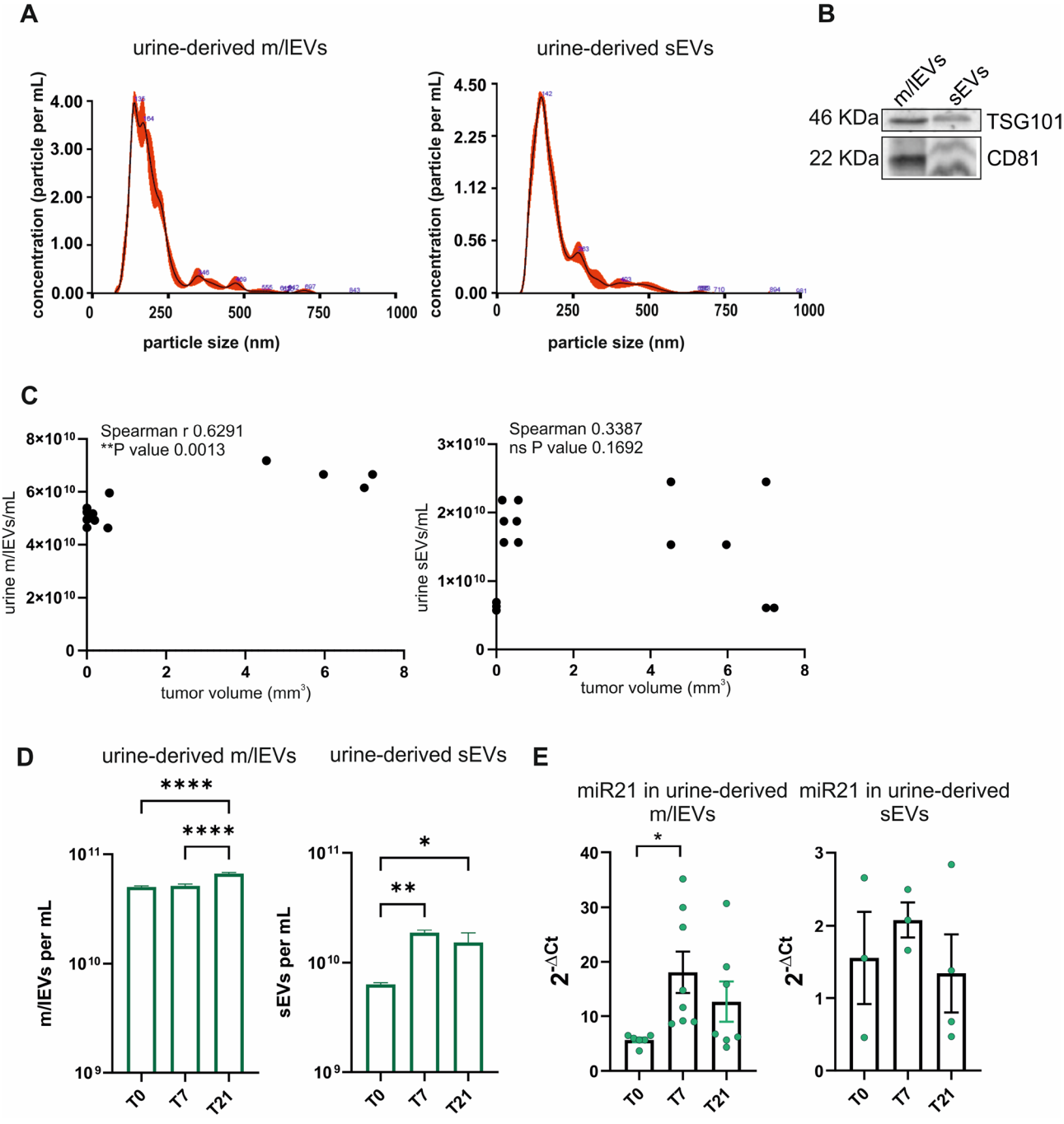

Fig. 3 EVs analysis in urine of GL261-bearing mice. **A** Representative concentration/size graphs from the nanoparticle tracking analysis (NTA). The average concentration (mean ± SE; in particles/mL) and mean size (± SE; in nm) of m/lEVs (left panel) and sEVs (right panel) isolated from urine of GL261-bearing mice. **B** Western blotting on m/lEVs and sEVs isolated from urine of GL261-bearing mice, CD81 and TSG101 are used as EVs markers. **C** Concordance between tumor size and the m/lEV and sEVs release in urine identified using Spearman nonparametric correlation analysis; two-tailed p values and *r* correlation coefficients are indicated. **D** Quantification of m/lEVs (left panel) and sEVs (right panel) isolated from urine of GL261-bearing mice time-dependent. Data are reported as mean ± SEM, *n* = 3/independent experiments, ANOVA one-way, Tukey's post-hoc analysis, *$p < 0.05$, ** $p < 0.001$, **** $p < 0.0001$. **E** Quantitative real-time PCR of miR21 expression in m/lEVs (left panel) and sEVs (right panel) isolated from urine of GL261-bearing mice at different time points (T0, T7, T21). Each sample has been normalized to U6 snRNA. Data were expressed as the mean ± SEM of $2^{-\Delta Ct}$, T0 = 3–6 animals, T7 = 3–8 animals, T21 = 4–7 animals. Data were analyzed with ANOVA one-way, Tukey's post-hoc analysis, * $p < 0.05$

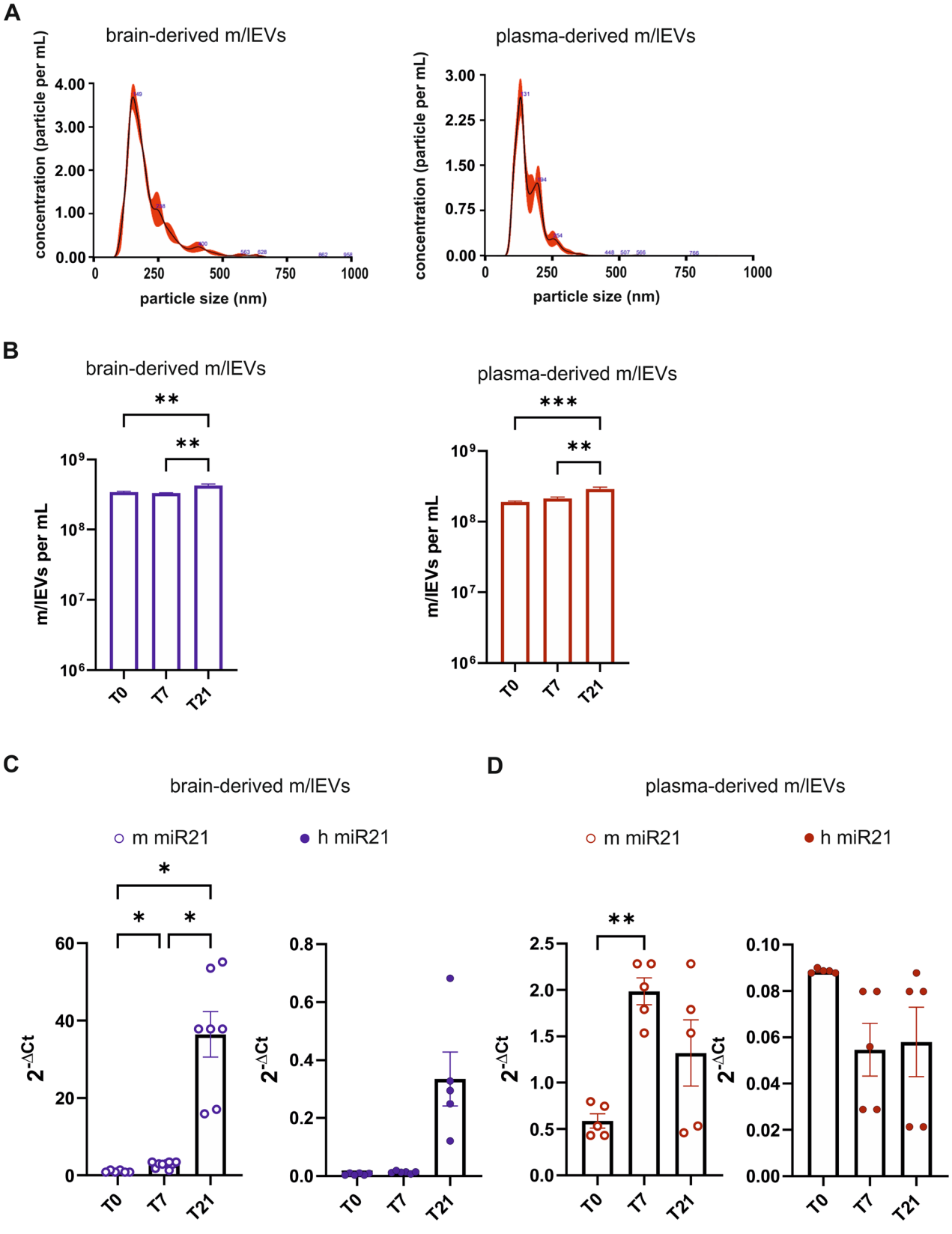

Fig. 4 (See legend on next page.)

(See figure on previous page.)

Fig. 4 miR21 expression in EVs from brain and plasma of U87MG-bearing mice. **A** Representative concentration/size graphs from the nanoparticle tracking analysis (NTA) on m/lEVs derived from brain and plasma of U87MG-bearing mice. **B** Quantification of m/lEVs isolated from brain and plasma of U87MG-bearing mice. Data are reported as mean ± SEM, $n = 4$/independent experiments, ANOVA one-way, Tukey's post-hoc analysis, ** $p < 0.01$. **C** Quantitative real-time PCR of miR21 expression in m/lEVs derived from murine (m_miR21, empty circles) and human part (h_miR21, filled circles) isolated from brain of U87MG-bearing mice at different time points (T0, T7, T21). Each sample has been normalized to U6 snRNA. Data were expressed as the mean ± SEM of $2^{-\Delta Ct}$, T0 = 6 animals, T7 = 6 animals, T21 = 6 animals. Data were analyzed by ANOVA one-way, Tukey's post-hoc analysis, * $p < 0.05$. **D** Quantitative real-time PCR of miR21 expression in m/lEVs derived from murine (m_miR21, empty circles) and human part (h_miR21, filled circles) isolated from plasma of U87MG-bearing mice at different time points (T0, T7, T21). Each sample has been normalized to U6 snRNA. Data were expressed as the mean ± SEM of $2^{-\Delta Ct}$, T0 = 5 animals, T7 = 5 animals, T21 = 5 animals. Data were analyzed by with ANOVA one-way, Tukey's post-hoc analysis, ** $p < 0.01$

not perform analyses at the same time points used for U87MG-inoculated SCID mice [46].

GCM-treated microglial cells release miR21 in vitro

To better investigate the role of cells of the TME in releasing miR21-containing EVs, we took advantage of in vitro experiments. Primary microglial or astrocytic cells were stimulated for 24 h with GL261-conditioned medium (GCM). After a 24 h-change medium, m/lEVs were isolated [27, 28] and data shown in Figs. 5A, B demonstrate an increase of miR21 in m/lEVs only in GCM-stimulated microglial cells. In line with the previous observation suggesting a non-tumoral origin of miR21, GL261 cells were pre-treated with a specific miR21 inhibitor ([54] and Figs. 5C, D) before GCM transfer to microglial cells (BV2). Indeed, Fig. 5E demonstrate that this treatment did not reduce (but rather increased) miR21 in BV2-derived m/lEVs [55].

Discussion

In this study we investigated the potential of EVs as early biomarkers for glioma diagnosis using biofluids. miR21 is a well-established early oncogenic marker, already demonstrated in the context of several tumors such as breast, lung, and colorectal cancer [56–58]. However, the novelty of our findings lies in the possibility of using miR21 as an early biomarker in glioblastoma, tumor that lacks any early diagnostic tools. Our findings revealed that miR21 is overexpressed in m/lEVs derived from the brain, plasma, and urine of glioma-bearing mice in early phase of glioma growth. We demonstrate that, few days after glioma injection, EV-containing miR21 originates from non-tumoral cells, as shown by the amplification of murine miR21 in fluids derived from xenogeneic glioma model. At later time points, human miR21, specifically expressed by glioma cells is detected in EVs isolated from both brain tissue and biofluids, indicating a shift toward a tumor-derived source. This distinction was made possible by using specie-specific primers in the U87MG xenograft model, allowing to differentiate between host and tumor-derived miR21.

Investigating the early origin of miR21 in glioma could help to understand the role of EVs in mediating miRNA transfer among tumor cells and the tumor microenvironment [59, 60]. It has been reported that glioma-derived EVs enriched in miR21 are transferred to microglial cells, affecting cell reprogramming toward a pro-tumor phenotype, increasing proliferation and the expression of genes which promote tumor progression [3, 44]. In contrast, a direct microglial origin of miR21 in glioma has never been described. Our data indicate a clear enrichment of miR21 in m/lEVs released by microglial cells; however, this observation was obtained in vitro and therefore requires further validation. Future experiments will be necessary to demonstrate whether the early increase of miR21 observed in plasma and urine EVs in glioma-bearing mice in vivo may indeed result from early microglial activation in response to tumor cell presence.

Our observation that in the xenogeneic mouse model the EV-miR21 derives from the host (mouse) tissue at 7 days from tumor injection, lead us to speculate that this could be a common mechanism also in the syngeneic model, supporting the non-tumoral origin of the increased miR21. This is supported by in vitro experiments, where 24 h of GCM stimulation specifically increased the release of miR21 containing EVs from microglial cells, not from astrocytes. Of course, these data do not exclude a later glioma-to-microglia transfer of miR21 also in our system [11]. Even if our in vitro results suggest that microglia could be a primary source of miR21-EV in glioma bearing mice, we cannot exclude the contribution of other non-tumoral cells, such as neurons and/or infiltrating immune cells.

Importantly, we focused our main analysis on m/lEVs, as these vesicles showed a consistent and early increase in miR21 across brain, plasma, and urine samples. In contrast, sEVs did not exhibit the same early enrichment in miR21. These differences may reflect distinct biogenesis pathways, cargo loading mechanisms, and cellular origins, which could influence their diagnostic potential. Future studies will be needed to better characterize these differences and their relationship with specific miRNA content and functional roles in glioma initiation process.

EV-miR21 has emerged as a promising non-invasive biomarker for various cancers by showing high sensitivity and specificity across multiple tumor types and biofluids, including brain tissue, plasma, and urine [61]. Concerning brain tumors, while several studies have reported elevated levels of miR21 in the plasma [62] and cerebrospinal fluid [11] of patients, a comparable early

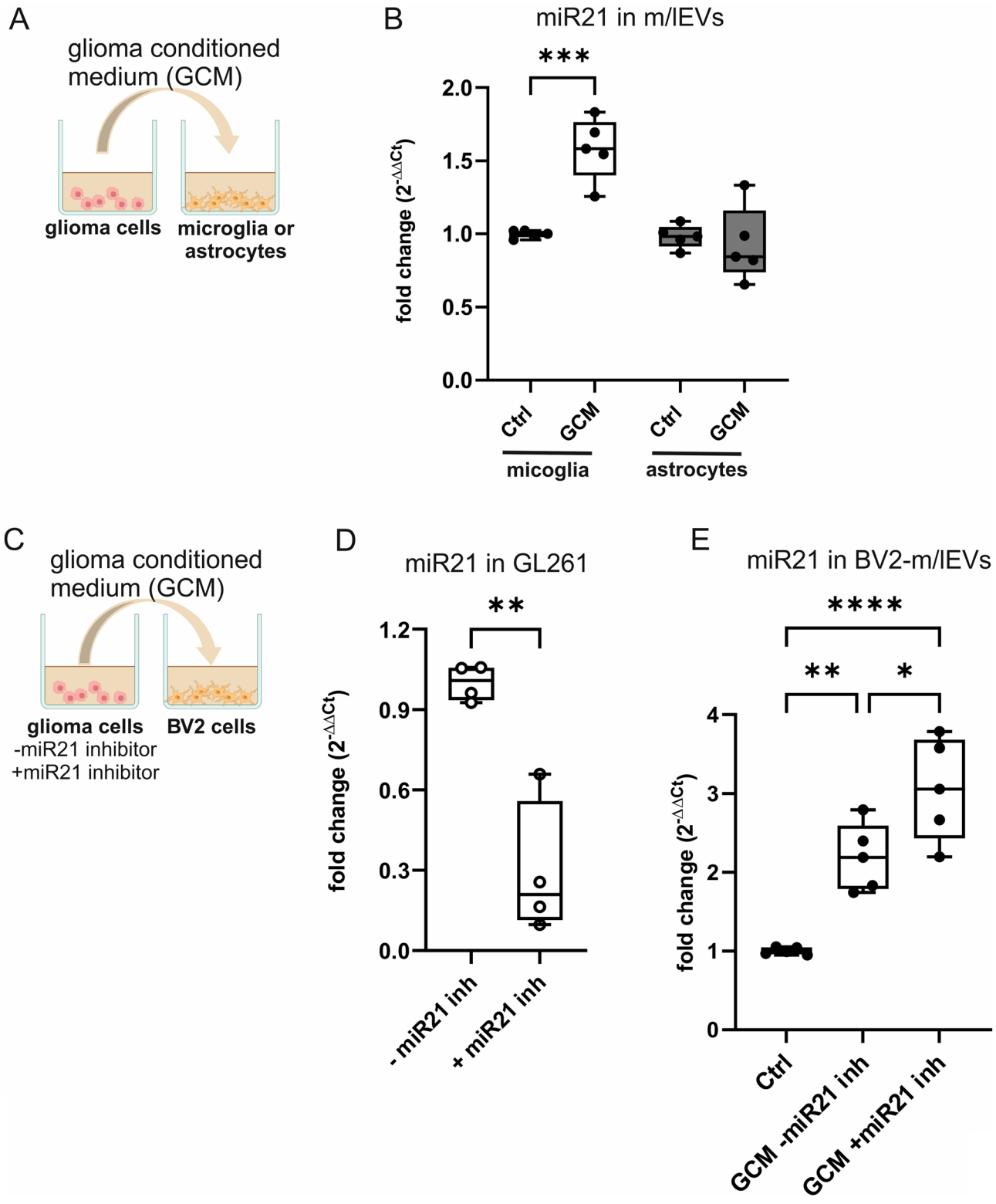

Fig. 5 (See legend on next page.)

(See figure on previous page.)

Fig. 5 miR21 expression in m/lEVs released by GCM-treated glial cells in vitro. **A** Experimental scheme: primary microglial or astrocytic cells were stimulated with GCM isolated from GL261 cells (GCM). **B** Quantitative real-time PCR of miR21 expression in m/lEVs isolated from supernatant of primary microglial and astrocytic cells upon 24 h stimulus of GCM. GCM group was compared to control group (cells not treated with GCM, Ctrl). Data were expressed as the mean ± SEM of 2^(−ΔΔCt), $n = 5$/experimental group. Each sample has been normalized to U6 snRNA. Data were analyzed by ANOVA one-way, Tukey's post-hoc analysis, ***$p < 0.001$. **C** Experimental scheme: BV2 microglial-like cells were stimulated with GCM isolated from GL261 cells transfected with vehicle (-) or miR21 inhibitor (+). **D** Quantitative real-time PCR of miR21 expression in GL261 cells transfected with vehicle (-) or miR21 inhibitor (+) $n = 4$/experimental group. Each sample has been normalized to U6 snRNA. Data were expressed as the mean ± SEM of fold change (2^(−ΔΔCt)). Data were analyzed by unpaired t-test, ** $p < 0.001$. **E** Quantitative real-time PCR of miR21 expression in m/lEVs released by BV2 cells unstimulated (Ctrl) or stimulated with GCM from GL261 transfect with vehicle (-) or from GL261 transfected with miR21 inhibitor (+). Data were expressed as the mean ± SEM of 2^(−ΔΔCt), $n = 5$/experimental group. Each sample has been normalized to U6 snRNA. Data were analyzed by ANOVA one-way, Tukey's post-hoc analysis, * $p < 0.05$, ** $p < 0.01$, **** $p < 0.0001$

and coordinated increase across brain, plasma, and urine EVs has not been clearly demonstrated in the clinical setting. Respect to the urine samples, miR21 has been found to be upregulated in urinary EVs in other tumor types, including colerectal, prostate, and urothelial cancers [63–65], where it has shown potential as a non-invasive biomarker for diagnosis and prognosis. These findings support the broader relevance of miR21 in cancer biology and highlight the need for comparative analyses with existing datasets [66] to validate the translational potential of our results in glioma.

miR21 overexpression was not observed in m/lEVs isolated from plasma at later stages in PDOX GBM mouse models. We speculate that these differences could be explained by a different cross talk between mouse host cells and human tumour cells. We must also consider that the different PDOX models reflect different GBM phenotypes; the angiogenic P13 has been associated with a partially disrupted BBB at late tumor stage [39, 40] and different amount of human miR21 is observed when compared to P8 bearing mice (albeit not significant).

Interestingly, the increase in miR21 in plasma m/lEVs observed in this study may reflect the molecular changes that occur in the brain during the early stages of tumorigenesis. This supports the idea that circulating EVs, like other circulating biomarkers, may act as a 'window' into the brain tumour microenvironment, providing an opportunity for early diagnosis and prognosis, and for monitoring drug responses and development of targeted therapies using minimally invasive liquid biopsies. Even if we assume that the increase observed in plasma and urine reflects changes occurring in the brain, it cannot be ruled out that these increases may occur independently of the processes observed in the brain and/or in isolated brain cells. Further studies are needed to validate these findings in patient biofluids, including standardisation of EV isolation and miR21 detection techniques.

Limits of the study

Despite the promising results, our study presents two important limitations already discussed; first, while our data suggest that microglial cells may be a primary source of miR21-enriched EVs in the early stages of glioma, we cannot exclude the contribution of other non-tumoral cell types; second, the EVs isolated from the plasma of glioma-bearing mice likely originate from a heterogeneous population of cells. Future in-depth studies will aim to sort plasma-derived EVs to selectively isolate those released by microglial cells, in order to more robustly support the hypothesis of their contribution to miR21 expression in vivo. Additionally, differences observed in PDOX models may reflect not only tumor heterogeneity but also species-specific interactions between human tumor cells and the murine host microenvironment. Finally, further validation in patient-derived biofluids and standardization of EV isolation and miRNA quantification methods as well as comparative profiling of EV-miRNAs across different biofluids and EV subtypes are essential to confirm the translational relevance of our findings.

Conclusions

In conclusion, the results obtained in this study confirm the importance of miR21 as glioma marker, highlighting its role as an early indicator of the disease, specifically produced by cells of non-tumoral origin, likely perturbed by the early glioma cell growth. These data suggest that miR21 in EVs released by non-tumoral cells and isolated from liquid biopsies, could enable early diagnosis or recurrence.

Abbreviations

ANOVA	Analysis of variance
BBB	Blood brain barrier
BCL-XL	B-cell lymphoma-extra large
BTG2	B-cell translocation gene 2
CSF	Cerebrospinal fluid
EGRFvIII	Epidermal growth factor receptor variant III
EVs	Extracellular vesicles
FPKM	Fragments per kilobase per million
GBM	Glioblastoma multiforme
GCM	Glioma-conditioned medium
IKK	IkappaB kinase
IL-6	Interleukin 6
IL-8	Interleukin 8
miR	MicroRNA
m/lEVs	Medium/large extracellular vesicles
MRI	Magnetic resonance imaging
NTA	Nanoparticle tracking analysis
OCT	Optimal cutting temperature
PD-L1	Programmed death-ligand 1

PDOX	Patient-derived orthotopic xenograft
PFA	Paraformaldehyde
PI3K/AKT	Phosphoinositide 3-kinase/KT
PTEN	Phosphatase and tensin homolog
qRT-PCR	Quantitative reverse tramscription- polymerase chain reaction
SCID mice	Severe combined immunodeficient mice
SEM	Standard error of the mean
sEVs	Small extracellular vesicles

Supplementary Information

The online version contains supplementary material available at https://doi.org/10.1186/s12974-025-03605-1.

Supplementary Material 1.

Supplementary Material 2.

Acknowledgements
We would like to thank Ms Amandine Bernard for the technical support with the analyses conducted in the PDOXs.
We would like to thank Plaisant Srl for contribution with its facilities and expertise for the collection of urine samples from mice.

Authors' contributions
MDL: Software, Methodology, Investigation, Formal analysis. AR: Software, Methodology, Investigation, Formal analysis. AI: Methodology, Investigation. AO: Methodology, Investigation. AS: Methodology, Investigation. AP: Methodology, Investigation. LV: Methodology, Investigation. AG: Writing – review & editing, Supervision. IDA: Investigation, Formal analysis. AM: Writing – review & editing, Supervision. CL: Writing – review & editing, Writing – original draft, Supervision, Project administration, Funding acquisition, Conceptualization. MC: Writing – review & editing, Writing – original draft, Validation, Supervision, Resources, Project administration, Methodology, Funding acquisition, Formal analysis, Data curation, Conceptualization.

Funding
This work was supported by Italian Ministry of Health (PNC SALUTE – D3 4 Health – Digital Driven Diagnostics, prognostics and therapeutics for sustainable Health care – PNC0001, Spoke 3 Linea tematica 2, CUP B53C22006120001 to C.L.); Italian Ministry of University and Research (PRIN-PNRR-P2022×5ESC to C.L.); by Associazione Italiana per la Ricerca sul Cancro (AIRC2019-IG23010) to C.L.; Italian Ministry of Health (PON "RICERCA E INNOVAZIONE" 2014–2020 - AZIONE IV.4 "DOTTORATI E CONTRATTI DI RICERCA SU TEMATICHE DELL'INNOVAZIONE") to M.C; Sapienza University of Rome (RG123188B4236B9C) to M.C.

Data availability
No datasets were generated or analysed during the current study.

Declarations

Ethics approval and consent to participate
Not applicable.

Consent for publication
Not applicable.

Competing interests
The authors declare no competing interests.

Author details
[1]Department of Physiology and Pharmacology, Sapienza University of Rome, Rome 00185, Italy
[2]NORLUX Neuro-Oncology Laboratory, Department of Cancer Research, Luxembourg Institute of Health, Luxembourg L-1210, Luxembourg
[3]Neuro-Immunology Group, Department of Cancer Research, Luxembourg Institute of Health, Luxembourg L-1210, Luxembourg
[4]Institute of Biomedical Technologies, CNR, Segrate, MI 20054, Italy
[5]Department of Physiology and Pharmacology, Laboratory Affiliated to Istituto Pasteur Italia Fondazione Cenci Bolognetti, Sapienza University, Rome, 00185, Italy
[6]IRCCS Neuromed, Pozzilli, IS 86077, Italy

Received: 24 June 2025 / Accepted: 20 October 2025
Published online: 02 December 2025

References

1. Jiang H, Yu K, Li M, Cui Y, Ren X, Yang C, Zhao X, Lin S. Classification of progression patterns in glioblastoma: analysis of predictive factors and clinical implications. Front Oncol. 2020. https://doi.org/10.3389/fonc.2020.590648.
2. Vecht CJ, Kerkhof M, Duran-Pena A. Seizure prognosis in brain tumors: new insights and evidence-based management. Oncologist. 2014. https://doi.org/10.1634/theoncologist.2014-0060.
3. Yuile P, Dent O, Cook R, Biggs M, Little N. Survival of glioblastoma patients related to presenting symptoms, brain site and treatment variables. J Clin Neurosci. 2006. https://doi.org/10.1016/j.jocn.2005.10.011.
4. Rapp M, Baernreuther J, Turowski B, Steiger HJ, Sabel M, Kamp MA. Recurrence pattern analysis of primary glioblastoma. World Neurosurg. 2017. https://doi.org/10.1016/j.wneu.2017.04.053.
5. Bauman MMJ, Bouchal SM, Monie DD, Aibaidula A, Singh R, Parney IF. Strategies, considerations, and recent advancements in the development of liquid biopsy for glioblastoma: a step towards individualized medicine in glioblastoma. Neurosurg Focus. 2022. https://doi.org/10.3171/2022.9.FOCUS22430.
6. Valadi H, Ekström K, Bossios A, Sjöstrand M, Lee JJ, Lötvall JO. Exosome-mediated transfer of mRNAs and MicroRNAs is a novel mechanism of genetic exchange between cells. Nat Cell Biol. 2007. https://doi.org/10.1038/ncb1596.
7. Li SR, Man QW, Gao X, Lin H, Wang J, Su FC, Wang HQ, Bu LL, Liu B, Chen G. Tissue-derived extracellular vesicles in cancers and non-cancer diseases: present and future. J Extracell Vesicles. 2021. https://doi.org/10.1002/jev2.12175.
8. Skog J, Würdinger T, van Rijn S, Meijer DH, Gainche L, Sena-Esteves M, et al. Glioblastoma microvesicles transport RNA and proteins that promote tumour growth and provide diagnostic biomarkers. Nat Cell Biol. 2008. https://doi.org/10.1038/ncb1800.
9. Mondal A, Kumari Singh D, Panda S, Shiras A. Extracellular vesicles as modulators of tumor microenvironment and disease progression in glioma. Front Oncol. 2017. https://doi.org/10.3389/fonc.2017.00144.
10. Low JJW, Sulaiman SA, Johdi NA, Abu N. Immunomodulatory effects of extracellular vesicles in glioblastoma. Front Cell Dev Biol. 2022. https://doi.org/10.3389/fcell.2022.996805.
11. Akers JC, Ramakrishnan V, Kim R, Skog J, Nakano I, Pingle S, et al. MiR-21 in the extracellular vesicles (EVs) of cerebrospinal fluid (CSF): a platform for glioblastoma biomarker development. PLoS ONE. 2013. https://doi.org/10.1371/journal.pone.0078115.
12. Manterola L, Guruceaga E, Gallego Perez-Larraya J, Gonzalez-Huarriz M, Jauregui P, Tejada S, et al. A small noncoding RNA signature found in exosomes of GBM patient serum as a diagnostic tool. Neuro Oncol. 2014. https://doi.org/10.1093/neuonc/not218.
13. Ricklefs FL, Wollmann K, Salviano-Silva A, Drexler R, Maire CL, Kaul MG, et al. Circulating extracellular vesicles as biomarker for diagnosis, prognosis, and monitoring in glioblastoma patients. Neuro Oncol. 2024;26(7):1280–91. https://doi.org/10.1093/neuonc/noae068.
14. Deregibus MC, Cantaluppi V, Calogero R, Lo Iacono M, Tetta C, Biancone L, et al. Endothelial progenitor cell derived microvesicles activate an angiogenic program in endothelial cells by a horizontal transfer of mRNA. Blood. 2007. https://doi.org/10.1182/blood-2007-03-078709.
15. Donnini S, Ziche M. Constitutive and inducible nitric oxide synthase: role in angiogenesis. Antioxid Redox Signal. 2002. https://doi.org/10.1089/152308602760598972.
16. Shiojima I, Walsh K. Role of Akt signaling in vascular homeostasis and angiogenesis. Circ Res. 2002. https://doi.org/10.1161/01.res.0000022200.71892.9f.
17. Chen RQ, Liu F, Qiu XY, Chen XQ. The prognostic and therapeutic value of PD-L1 in glioma. Front Pharmacol. 2019. https://doi.org/10.3389/fphar.2018.01503.
18. Wu P, Guo Y, Xiao L, Yuan J, Tang C, Dong J, Qian Z. Correction to: LILRB2-containing small extracellular vesicles from glioblastoma promote tumor progression by promoting the formation and expansion of myeloid-derived

suppressor cells. Cancer Immunol Immunother. 2023. https://doi.org/10.1007/s00262-023-03426-2.
19. Antonios JP, Soto H, Everson RG, Moughon D, Orpilla JR, Shin NP, et al. Immunosuppressive tumor-infiltrating myeloid cells mediate adaptive immune resistance via a PD-1/PD-L1 mechanism in glioblastoma. Neuro Oncol. 2017. https://doi.org/10.1093/neuonc/now287.
20. Xu H, Li M, Pan Z, Zhang Z, Gao Z, Zhao R, et al. miR-3184-3p enriched in cerebrospinal fluid exosomes contributes to progression of glioma and promotes M2-like macrophage polarization. Cancer Sci. 2022. https://doi.org/10.1111/cas.15372.
21. Li M, Xu H, Qi Y, Pan Z, Li B, Gao Z, et al. Tumor-derived exosomes deliver the tumor suppressor miR-3591-3p to induce M2 macrophage polarization and promote glioma progression. Oncogene. 2022. https://doi.org/10.1038/s41388-022-02457-w.
22. Qian M, Wang S, Guo X, Wang J, Zhang Z, Qiu W, et al. Hypoxic glioma-derived exosomes deliver microRNA-1246 to induce M2 macrophage polarization by targeting TERF2IP via the STAT3 and NF-κB pathways. Oncogene. 2020. https://doi.org/10.1038/s41388-019-0996-y.
23. Pan Z, Zhao R, Li B, Qi Y, Qiu W, Guo Q, et al. EWSR1-induced circNEIL3 promotes glioma progression and exosome-mediated macrophage immunosuppressive polarization via stabilizing IGF2BP3. Mol Cancer. 2022. https://doi.org/10.1186/s12943-021-01485-6.
24. Zhang L, Zhang S, Yao J, Lowery FJ, Zhang Q, Huang WC, et al. Microenvironment-induced PTEN loss by Exosomal MicroRNA primes brain metastasis outgrowth. Nature. 2015. https://doi.org/10.1038/nature15376.
25. Gao Y, Ma H, Lv C, Lan F, Wang Y, Deng Y. Exosomes and Exosomal MicroRNA in non-targeted radiation bystander and abscopal effects in the central nervous system. Cancer Lett. 2021. https://doi.org/10.1016/j.canlet.2020.10.049.
26. Azam Z, Quillien V, Wang G, To ST. The potential diagnostic and prognostic role of extracellular vesicles in glioma: current status and future perspectives. Acta Oncol. 2019. https://doi.org/10.1080/0284186X.2018.1551621.
27. Serpe C, Michelucci A, Monaco L, Rinaldi A, De Luca M, Familiari P, Relucenti M, Di Pietro E, Di Castro MA, D'Agnano I, Catacuzzeno L, Limatola C, Catalano M. Astrocytes-Derived small extracellular vesicles hinder glioma growth. Biomedicines. 2022;10(11):2952. https://doi.org/10.3390/biomedicines10112952.
28. Grimaldi A, Serpe C, Chece G, Nigro V, Sarra A, Ruzicka B, Relucenti M, Familiari G, Ruocco G, Pascucci GR, Guerrieri F, Limatola C, Catalano M. Microglia-Derived microvesicles affect microglia phenotype in glioma. Front Cell Neurosci. 2019;13:41. https://doi.org/10.3389/fncel.2019.00041.
29. Serpe C, Monaco L, Relucenti M, Iovino L, Familiari P, Scavizzi F, Raspa M, Familiari G, Civiero L, D'Agnano I, Limatola C, Catalano M. Microglia-Derived small extracellular vesicles reduce glioma growth by modifying tumor cell metabolism and enhancing glutamate clearance through miR-124. Cells. 2021;10(8):2066. https://doi.org/10.3390/cells10082066.
30. Feng YH, Tsao CJ. Emerging role of microRNA-21 in cancer. Biomed Rep. 2016. https://doi.org/10.3892/br.2016.747.
31. Møller HG, Rasmussen AP, Andersen HH, Johnsen KB, Henriksen M, Duroux M. A systematic review of MicroRNA in glioblastoma multiforme: micro-modulators in the mesenchymal mode of migration and invasion. Mol Neurobiol. 2013. https://doi.org/10.1007/s12035-012-8349-7.
32. Ciafrè SA, Galardi S, Mangiola A, Ferracin M, Liu CG, Sabatino G, Negrini M, Maira G, Croce CM, Farace MG. Extensive modulation of a set of MicroRNAs in primary glioblastoma. Biochem Biophys Res Commun. 2005. https://doi.org/10.1016/j.bbrc.2005.07.030.
33. Teplyuk NM, Mollenhauer B, Gabriely G, Giese A, Kim E, Smolsky M, et al. MicroRNAs in cerebrospinal fluid identify glioblastoma and metastatic brain cancers and reflect disease activity. Neuro Oncol. 2012. https://doi.org/10.1093/neuonc/nos074.
34. Asangani IA, Rasheed SA, Nikolova DA, Leupold JH, Colburn NH, Post S, Allgayer H. MicroRNA-21 (miR-21) post-transcriptionally downregulates tumor suppressor Pdcd4 and stimulates invasion, intravasation and metastasis in colorectal cancer. Oncogene. 2008;27(15):2128–36. https://doi.org/10.1038/sj.onc.1210856.
35. Kwak HJ, Kim YJ, Chun KR, Woo YM, Park SJ, Jeong JA. et. al. Downregulation of Spry2 by miR-21 triggers malignancy in human gliomas. Oncogene. 2011;30(21):2433–42. https://doi.org/10.1038/onc.2010.620.
36. Xue X, Liu Y, Wang Y, Meng M, Wang K, Zang X, et al. MiR-21 and MiR-155 promote non-small cell lung cancer progression by downregulating SOCS1, SOCS6, and PTEN. Oncotarget. 2016;7(51):84508–19. https://doi.org/10.18632/oncotarget.13022.
37. Leite KR, Reis ST, Viana N, Morais DR, Moura CM, Silva IA, et al. Controlling RECK miR21 promotes tumor cell invasion and is related to biochemical recurrence in prostate cancer. J Cancer. 2015;6(3):292–301. https://doi.org/10.7150/jca.11038.
38. Hatley ME, Patrick DM, Garcia MR, Richardson JA, Bassel-Duby R, van Rooij E, Olson EN. Modulation of K-Ras-dependent lung tumorigenesis by MicroRNA-21. Cancer Cell. 2010;18(3):282–93. https://doi.org/10.1016/j.ccr.2010.08.013.
39. Chi LH, Cross RSN, Redvers RP, Davis M, Hediyeh-Zadeh S, Mathivanan S, et al. MicroRNA-21 is immunosuppressive and pro-metastatic via separate mechanisms. Oncogenesis. 2022. https://doi.org/10.1038/s41389-022-00413-7.
40. Meng G, Wei J, Wang Y, et al. miR-21 regulates immunosuppression mediated by myeloid-derived suppressor cells by impairing RUNX1-YAP interaction in lung cancer. Cancer Cell Int. 2020;20:495. https://doi.org/10.1186/s12935-020-01555-7.
41. Lakomy R, Sana J, Hankeova S, Fadrus P, Kren L, Lzicarova E, et al. MiR-195, miR-196b, miR-181c, miR-21 expression levels and O-6-methylguanine-DNA methyltransferase methylation status are associated with clinical outcome in glioblastoma patients. Cancer Sci. 2011. https://doi.org/10.1111/j.1349-7006.2011.02092.x.
42. Chuang HY, Su YK, Liu HW, Chen CH, Chiu SC, Cho DY, et al. Preclinical evidence of STAT3 inhibitor Pacritinib overcoming Temozolomide resistance via downregulating miR-21-Enriched exosomes from M2 Glioblastoma-Associated macrophages. J Clin Med. 2019;8(7):959. https://doi.org/10.3390/jcm8070959.
43. van der Vos KE, Abels ER, Zhang X, Lai C, Carrizosa E, Oakley D, et al. Directly visualized glioblastoma-derived extracellular vesicles transfer RNA to microglia/macrophages in the brain. Neuro Oncol. 2016. https://doi.org/10.1093/neuonc/nov244.
44. Abels ER, Maas SLN, Nieland L, Wei Z, Cheah PS, Tai E, et al. Glioblastoma-Associated microglia reprogramming is mediated by functional transfer of extracellular miR-21. Cell Rep. 2019. https://doi.org/10.1016/j.celrep.2019.08.036.
45. Sun X, Ma X, Wang J, Zhao Y, Wang Y, Bihl JC, et al. Glioma stem cells-derived exosomes promote the angiogenic ability of endothelial cells through miR-21/VEGF signal. Oncotarget. 2017. https://doi.org/10.18632/oncotarget.16661.
46. Oudin A, Baus V, Barthelemy V, Fabian C, Klein E, Dieterle M, et al. Protocol for derivation of organoids and patient-derived orthotopic xenografts from glioma patient tumors. STAR Protoc. 2021. https://doi.org/10.1016/j.xpro.2021.100534.
47. Yabo YA, Moreno-Sanchez PM, Pires-Afonso Y, Kaoma T, Nosirov B, Scafidi A, et al. Glioblastoma-instructed microglia transition to heterogeneous phenotypic States with phagocytic and dendritic cell-like features in patient tumors and patient-derived orthotopic xenografts. Genome Med. 2024. https://doi.org/10.1186/s13073-024-01321-8.
48. Lauro C, Cipriani R, Catalano M, Trettel F, Chece G, Brusadin V, et al. Adenosine A1 receptors and microglial cells mediate CX3CL1-induced protection of hippocampal neurons against Glu-induced death. Neuropsychopharmacology. 2010. https://doi.org/10.1038/npp.2010.26.
49. Catalano M, Lauro C, Cipriani R, Chece G, Ponzetta A, Di Angelantonio S, et al. CX3CL1 protects neurons against excitotoxicity enhancing GLT-1 activity on astrocytes. J Neuroimmunol. 2013. https://doi.org/10.1016/j.jneuroim.2013.07.020.
50. Crescitelli R, Lässer C, Lötvall J. Isolation and characterization of extracellular vesicle subpopulations from tissues. Nat Protoc. 2021. https://doi.org/10.1038/s41596-020-00466-1.
51. Théry C, Amigorena S, Raposo G, Clayton A. Isolation and characterization of exosomes from cell culture supernatants and biological fluids. Curr Protoc Cell Biol. 2006. https://doi.org/10.1002/0471143030.cb0322s30.
52. Livak KJ, Schmittgen TD. Analysis of relative gene expression data using real-time quantitative PCR and the 2(-Delta delta C(T)) method. Methods. 2001. https://doi.org/10.1006/meth.2001.1262.
53. Xu D, Di K, Fan B, Wu J, Gu X, Sun Y, et al. MicroRNAs in extracellular vesicles: sorting mechanisms, diagnostic value, isolation, and detection technology. Front Bioeng Biotechnol. 2022. https://doi.org/10.3389/fbioe.2022.948959.
54. Seo YE, Suh HW, Bahal R, Josowitz A, Zhang J, Song E, et al. Nanoparticle-mediated intratumoral Inhibition of miR-21 for improved survival in glioblastoma. Biomaterials. 2019. https://doi.org/10.1016/j.biomaterials.2019.02.016.
55. Rinaldi A, Balietti M, Principi E, De Luca M, De Felice E, Narcisi FM, et al. BV2-derived extracellular vesicles modulate microglia inflammatory profile,

neuronal plasticity, and behavioural performances in late adult mice. Brain Behav Immun. 2024. https://doi.org/10.1016/j.bbi.2024.08.012.
56. Omarini C, Catani V, Mastrolia I, et al. Extracellular vesicles-derived miR-21 as a biomarker for early diagnosis and tumor activity in breast cancer subtypes. Biomark Res. 2025. https://doi.org/10.1186/s40364-025-00724-y.
57. Tian L, Shan W, Zhang Y, et al. Up-Regulation of miR-21 expression predicate advanced clinicopathological features and poor prognosis in patients with Non-Small cell lung cancer. Pathol Oncol Res. 2016. https://doi.org/10.1007/s12253-015-9979-7.
58. Toiyama Y, Takahashi M, Hur K, Nagasaka T, Tanaka K, Inoue Y, et al. Serum miR-21 as a diagnostic and prognostic biomarker in colorectal cancer. J Natl Cancer Inst. 2013. https://doi.org/10.1093/jnci/djt101.
59. Olioso D, Caccese M, Santangelo A, Lippi G, Zagonel V, Cabrini G, et al. Serum Exosomal microRNA-21, 222 and 124-3p as noninvasive predictive biomarkers in newly diagnosed High-Grade gliomas: A prospective study. Cancers (Basel). 2021. https://doi.org/10.3390/cancers13123006.
60. Singh A, Singh AK, Giri R, Kumar D, Sharma R, Valis M, et al. The role of microRNA-21 in the onset and progression of cancer. Future Med Chem. 2021. https://doi.org/10.4155/fmc-2021-0096.
61. Shi J. Considering Exosomal miR-21 as a biomarker for cancer. J Clin Med. 2016. https://doi.org/10.3390/jcm5040042.
62. Aran V, Lyra Miranda R, Heringer M, Carvalho da Fonseca AC, et al. Liquid biopsy evaluation of Circulating tumor DNA, miRNAs, and cytokines in meningioma patients. Front Neurol. 2024. https://doi.org/10.3389/fneur.2023.1321895.
63. Ellakwa DE, Mushtaq N, Khan S, Jabbar A, Abdelmalek MA, Wadan AS, et al. Molecular functions of MicroRNAs in colorectal cancer: recent roles in proliferation, angiogenesis, apoptosis, and chemoresistance. Naunyn Schmiedebergs Arch Pharmacol. 2024. https://doi.org/10.1007/s00210-024-03076-w.
64. Mharrach I, Tadlaoui KA, Aqerrout M, Laraqui A, Ameur A, El Ghazzaly A, et al. Diagnostic value of miR-21 and miR-221 as potential biomarkers for early diagnosis of prostate cancer. Mol Clin Oncol. 2025. https://doi.org/10.3892/mco.2025.2835.
65. Kehl A, Aupperle-Lellbach H, Brockmann M, Weyer AV, Appenzeller M, Steiger K. Utility of urinary MiRNA biomarkers for canine urothelial carcinoma diagnostics. Vet Sci. 2025. https://doi.org/10.3390/vetsci12070621.
66. Qu K, Lin T, Pang Q, Liu T, Wang Z, Tai M, et al. Extracellular miRNA-21 as a novel biomarker in glioma: evidence from meta-analysis, clinical validation and experimental investigations. Oncotarget. 2016. https://doi.org/10.18632/oncotarget.9188.

Publisher's note